Arabian Journal of Chemistry (2016) 9, S1349–S1356

King Saud University

Arabian Journal of Chemistry

www.ksu.edu.sa
www.sciencedirect.com

ORIGINAL ARTICLE

The influence of Fe^{2+} concentration and deposition time on the corrosion resistance of the electrodeposited zinc–nickel–iron alloys

M.M. Abou-Krisha *, F.H. Assaf, S.A. El-Naby

Faculty of Science, Chemistry Department, South Valley University, Qena 83523, Egypt

Received 19 August 2011; accepted 28 February 2012
Available online 7 March 2012

KEYWORDS

Electrodeposition;
Anomalous codeposition;
Surface morphology;
Corrosion resistance;
Ternary Zn–Ni–Fe alloy

Abstract Electrodeposition operating conditions for Zn–Ni–Fe alloys from sulfate baths and the corrosion resistance of the electrodeposited alloys were studied. The comparison between Zn–Ni and Zn–Ni–Fe alloys co-deposition revealed that the remarkable inhibition of Ni and Fe deposition takes place due to the presence of Zn^{2+} in the plating bath. The electrodeposition was performed on the steel substrate, under galvanostatic conditions, for varying Fe^{2+} bath concentrations and at different times. X-ray diffraction studies of the deposit showed the presence of Fe_3Ni_2 phase and γ-phase with a composition of Ni_2Zn_{11}. The obtained data also exposed that the corrosion resistance increases as a result of increasing Fe^{2+} concentration and deposition time. Investigation was carried out using cyclic voltammetry and galvastatic techniques for electrodeposition, while linear polarization resistance and anodic linear sweeping voltammetry techniques were used for corrosion study.

1. Introduction

The electrodeposition of alloys is of great interest, since binary or higher order alloys are frequently used in a variety of industrial applications, one of the first applications having been the electroforming of printing plates (Safranekv, 1986). It has been shown that zinc alloys can provide improved corrosion resistance compared to pure zinc in the protection of ferrous-based metals. The most common zinc alloys are zinc–nickel, zinc–cobalt and zinc–iron (Eliaz et al., 2010; Chitharanjan Hegde et al., 2010; Yogesha and Chitharanjan Hegde, 2011; Liu et al., 2011; Li et al., 2011; Vlad et al., 2011; Tian et al., 2011; Ortiz et al., 2009). Zn–Fe alloys have been used a lot recently, since they showed excellent corrosion resistance (due to the nature of the zinc–iron phase), good paintability, formability and weldability (due to the high hardness and melting point of the zinc–iron phase in comparison to pure zinc) and ease of formation of the coating (Zhang et al., 2001). Zn–Ni alloys have received more attention than other zinc alloy deposits because of their high degree of corrosion resistance and their mechanical properties (Eliaz et al., 2010; Chitharanjan Hegde et al., 2010; Ganesan et al., 2007). Although, the Zn–Ni alloy electrodeposits are mainly used as coating to improve the corrosion resistance of automobile steel

* Corresponding author.
E-mail address: m_abou_krisha@yahoo.com (M.M. Abou-Krisha).
Peer review under responsibility of King Saud University.

Production and hosting by Elsevier

http://dx.doi.org/10.1016/j.arabjc.2012.02.014
1878-5352

bodies (Ashassi-Sorkhabi et al., 2001), these coatings have been considered for several other applications such as electrocatalytic water electrolysis (Hu, 2000). This alloy is also considered as a viable alternative to cadmium for plating aircraft and commercial steel parts (Veeraraghavan et al., 2004). The Zn–Ni–Fe alloy is a relatively recent addition to the family of Zn alloys and very few papers are published on it. It has already been observed that the addition of Fe to Zn–Ni alloy led to the formation of a ternary Zn–Ni–Fe alloy, from chloride bath, which helped in improving the appearance of the alloy and increasing corrosion resistance of it (Younan and Oki, 1996). In addition, Zn–Ni–Fe alloy was used as electrodes for a hydrogen evolution reaction (Ananth and Parthasaradhy, 1997). It is well-known that these zinc–iron group alloys are anomalous in nature, as classified by Brenner (Brenner, 1963), i.e. the less noble metal Zn deposits preferentially as compared to the more noble metals like Ni or Fe.

In the present study, the collection of the properties of Zn–Ni and Zn–Fe alloys in one alloy (Zn–Ni–Fe alloy) and investigation of its corrosion resistance are the main goals. The present investigation, also, focuses on a parameter study of the electrodeposition operating conditions for Zn–Ni–Fe ternary alloys from the sulfate electrolyte. The effects of various deposition parameters like Fe^{2+} concentrations and deposition time on the deposit composition and its corrosion resistance are reported in this paper.

2. Experimental

The alloy electrodeposits are prepared from a three electrode cell system made of a steel rod of cross sectional area (0.196 cm^2) serving as the deposition substrate; a platinum sheet as counter electrode and the reference electrode was the Ag/AgCl electrode. Zinc–nickel–iron alloys were obtained from baths of composition: 0.1 M $ZnSO_4$, 0.1 M $NiSO_4$, 0.1 M $FeSO_4$, 0.2 M Na_2SO_4 and 0.01 M H_2SO_4. This solution is buffered by 0.2 M H_3BO_3 to always keep the pH close to 2.5. The electrolytes used for the electrodeposition of Zn–Ni–Fe alloys were freshly prepared using Analar grade chemicals without further purification and dissolved in appropriate amounts of double distilled water. All experiments have been carried out in duplicate; the measurements have shown good reproducibility. For a standard bath deposition, a series of experiments at different times were carried out and the relative standard deviation (RSD%) was found to be 3.5%, 5.2% and 4.3% for the Zn, Fe and Ni contents in the deposit, respectively.

Before each run, the cell was cleaned with chromic/sulfuric mixture, washed with first and second distilled water, filled with the 50 cm^3 of the electroplating solution of temperature 30.0 °C and was placed during the experiment in air thermostat to ensure the adjustment of temperature at 30.0 °C. The electrodeposition process was usually performed at pH = 2.5 and current density 5.0 mA cm^{-2} for 10 min. While investigating the influence of deposition time and iron concentration, the electroplating was carried out at different deposition times and Fe^{2+} concentrations.

For electrochemical methods (cyclic voltammetric behavior, galvanostatic measurements, linear polarization resistance and anodic linear sweeping voltammetry techniques) EG&G Potentiostat/Galvanostat Model 273A controlled by a PC using 352 corrosion software was used.

Anodic sweeping voltammetry analysis is employed effectively for the in situ characterization of the electrodeposition process and products of the galvanostatically obtained electrodeposits on the steel substrate. For anodic sweeping voltammetry the galvanostatic deposition was carried out for 10 min in order to obtain a thin deposit. The purpose of these measurements was to perform a qualitative analysis and not a quantitative one. The analysis was performed right after the galvanostatic depositions, in 0.5 M Na_2SO_4 + 0.05 M EDTA solution.

All cyclic voltammetry experiments were initiated at 0.0 V in negative direction and reversed at −1.2 V in positive direction at scan rate of 5 mV s^{-1}.

The surface morphology of the deposit was evaluated by a Scanning Electron Microscope (JSM- 5500 LV, SEM, JEOL, Japan). X-ray diffractometry (XRD) X'Pert Pro PANalytical was used to identify the phases of Zn–Ni–Fe alloys deposited. Steel and copper sheets cathodes, of widths 1.0 cm and 1.0 cm in length, were used for XRD and SEM analyses, and chemical analysis, respectively. To steel and copper sheets provided with a narrow strip of about 1 cm^2 area, clamp terminals were attached for electrical contact. In order to determine the percentage composition of the deposit, the deposit was stripped in 30% (v/v) HCl solution, then diluted with double distilled water up to 100 cm^3 and analyzed to ascertain the Zn, Ni and Fe contents in the deposited alloy using Atomic Absorption Spectroscopy (Variian SpectrAA 55).

The thicknesses were calculated as mentioned in Abou-Krisha (2005). The values of electrochemical corrosion measurements of the coatings, the corrosion potential E_{corr}, the corrosion current I_{corr} and the polarization resistance R_p were obtained and represented in Tables 1 and 2.

3. Results and discussion

3.1. Effect of Fe^{2+} concentration in the bath on Zn–Ni–Fe alloy deposition

Fig. 1 shows the cyclic voltammetry for the electrodeposition of Zn–Ni and Zn–Ni–Fe alloys on steel rod in bath solution at 30.0 °C. It is observed from the anodic part in the cyclic voltammograms, for Zn–Ni, that there are three peaks that correspond to the dissolution of the constituents of two phases, δ-phase (Ni_3Zn_{22}) and γ-phase (Ni_5Zn_{21}). The first and second anodic peaks correspond to the dissolution (dealloying) of Zn from δ- and γ-phases respectively. The third peak corresponds to the dissolution of Ni from its phases as reported earlier by Abou-Krisha (2005). However, for Zn–Ni–Fe, there are four anodic current peaks. The first anodic peak is attributed to the dissolution of zinc from pure Zn phase, while the second anodic peak corresponds to the dissolution of zinc from (γ-Ni_2Zn_{11}) phase. The third and fourth anodic peaks at −633 mV and −318 mV correspond to the dissolution of iron from Fe_3Ni_2 phase and nickel from its phases respectively, which was verified by XRD (Fig. 2).

The cathodic peak which starts at about −577 m V may be attributed to the co-deposition of sulfur, which was produced from the reduction of the sulfate group at the cathode due to the presence of H_2SO_4 (Abou-Krisha et al., 2008).

Zn–Ni–Fe alloys are electrodeposited on the steel rod cathode from the electrolytes with a variation of Fe^{2+} ion concen-

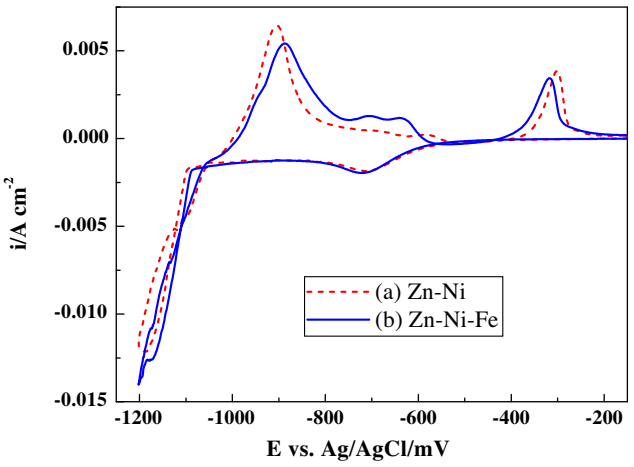

Figure 1 *i–E* curves (cyclic voltammograms) for steel in (a) 0.10 M $ZnSO_4$ and 0.10 M $NiSO_4$, (b) 0.10 M $ZnSO_4$, 0.10 M $NiSO_4$ and 0.10 M $FeSO_4$, with 0.01 M H_2SO_4, 0.20 M Na_2SO_4 and 0.20 M H_3BO_3 at scan rate 5 mV s^{-1} and 30 °C.

tration, ranging from 0.0 to 0.4 M using cyclic voltammetry, as shown in Fig. 3. It is clear that the cathodic peak current which is attributable to the formation of sulfur is slightly affected with increasing of Fe^{2+} ions concentration.

The anodic part of the cyclic voltammetry (Fig. 3) consists of four anodic peaks. The height of the first dissolution anodic peak which appears at −890 mV decreases with increasing Fe^{2+} concentration in the plating bath. The height of the second anodic peak at about −685 mV that appears at high Fe^{2+} concentration increases with increasing Fe^{2+}. The third peak at −614 mV appears only at higher iron ion concentration and increases with increasing its concentration, similar to the second peak. While the height of the anodic peak that appears at −317 mV increases with increasing of iron concentration and is shifted positively with further increasing of iron concentration. It was decided previously that the decreasing of Zn and increasing of Ni and Fe in the alloy lead to an increase in the corrosion resistance of the alloy (Abou-Krisha, 2005). Therefore, from the obtained results it is clear that the addition of Fe^{2+} to the bath lead to an increase in the corrosion resistance of the alloy.

The galvanostatic measurements for the deposition of Zn–Ni–Fe alloys on a steel rod were done (Fig. 4) to confirm the obtained results. There is some potential trembling, probably due to bubbles of hydrogen blocked partially on the electrode surface. In addition, inspection of the data reveals an appreciable decrease in cathodic deposition potential of the alloy when Fe^{2+} concentration increased in the plating bath. It was also observed that the curves approached the stationary values after initial times (nucleation stage). Therefore, the composition of deposited alloys remains unchanged during the growth of alloy deposit.

It is known that stripping methods are useful to determine the chemical and phase compositions of the alloys. In case of Zn–Ni–Fe alloy, in most conditions various peaks are observed in the oxidation scan that has been previously identified. The anodic linear sweep voltammograms (ALSV) obtained during the dissolution of the deposits (Fig. 5) show the influence of Fe^{2+} concentration on the phase structures of deposited Zn–Ni–Fe alloys. There are three anodic peaks corresponding to several phases in the alloy. These peaks correspond to the dissolution of zinc from the pure Zn phase (first peak). This peak is accompanied by the second anodic peak, which is attributed to the dissolution of zinc from (γ-Ni_2Zn_{11}) phase, which overlaps with the dissolution of iron from (Fe_3Ni_2) phase. The dissolution of nickel from its phases was characterized by the third anodic peak. These results revealed that, the additional increase in the corrosion resistance of Zn–Ni–Fe deposits is not only due to the formation of a high nickel γ-alloy phase but also due to the co-deposition of iron.

Fig. 6 shows linear polarization resistance tests, which have been done using steel-coated galvanostatically by Zn–Ni–Fe

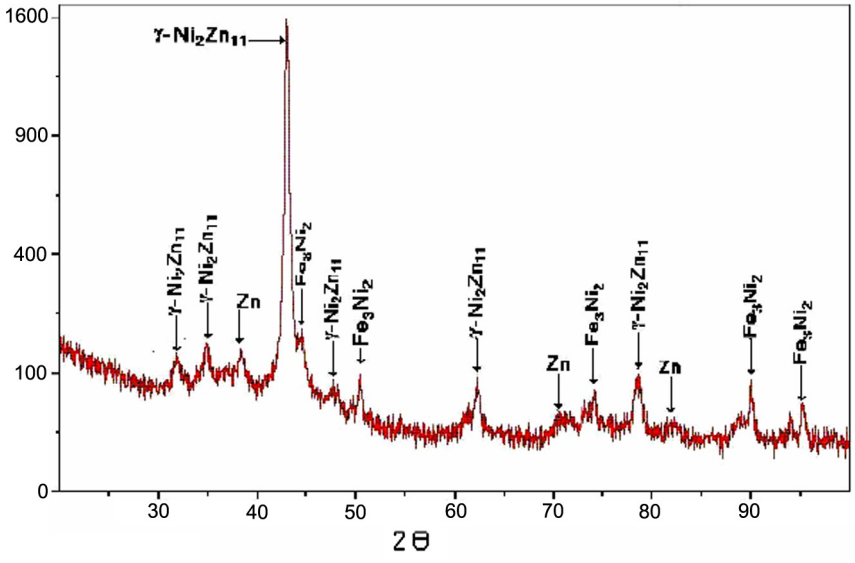

Figure 2 XRD patterns of electrodeposited Zn–Ni–Fe alloy on steel from a bath containing 0.10 M $ZnSO_4$, 0.10 M $FeSO_4$, 0.10 M $NiSO_4$, 0.01 M H_2SO_4, 0.20 M Na_2SO_4, 0.20 M H_3BO_3 at 5 mA cm^{-2} for 10 min at 30 °C.

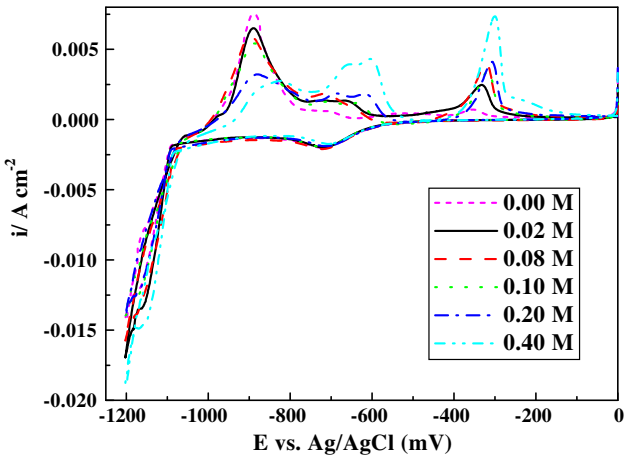

Figure 3 *i–E* curves (cyclic voltammograms) for steel in 0.10 M $ZnSO_4$, 0.10 M $NiSO_4$, 0.01 M H_2SO_4, 0.20 M Na_2SO_4 and 0.20 M H_3BO_3 with different concentrations of $FeSO_4$ and scan rate 5 mV s^{-1} at 30.0 °C.

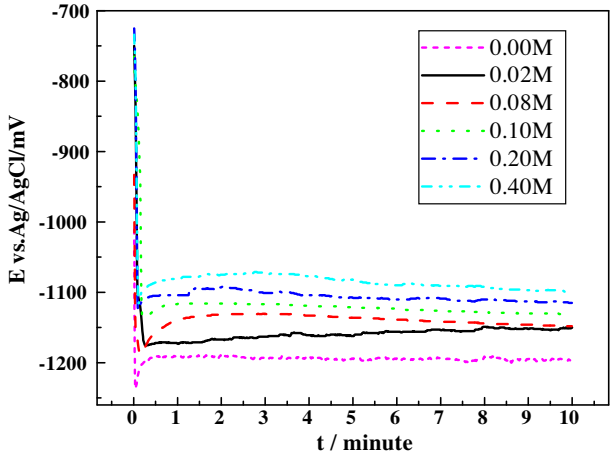

Figure 4 *E–t* curves for steel in 0.10 M $ZnSO_4$, 0.10 M $NiSO_4$, 0.01 M H_2SO_4, 0.20 M Na_2SO_4 and 0.20 M H_3BO_3 with different concentrations of $FeSO_4$ at 5 mA cm^{-2} for 10 min at 30.0 °C.

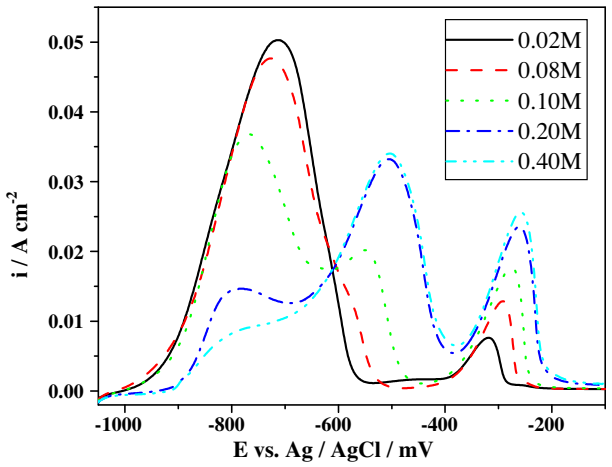

Figure 5 ALSVs of Zn–Ni–Fe alloy, electrodeposited on steel from a bath containing 0.10 M $ZnSO_4$, 0.10 M $NiSO_4$, 0.01 M H_2SO_4, 0.20 M Na2SO4, 0.20 M H_3BO_3 with different concentrations of $FeSO_4$ at 5 mA cm^{-2} for 10 min at 30.0 °C, in 0.5 M Na_2SO_4 + 0.05 M EDTA solution at scan rate 5 mV s^{-1} and 30 °C.

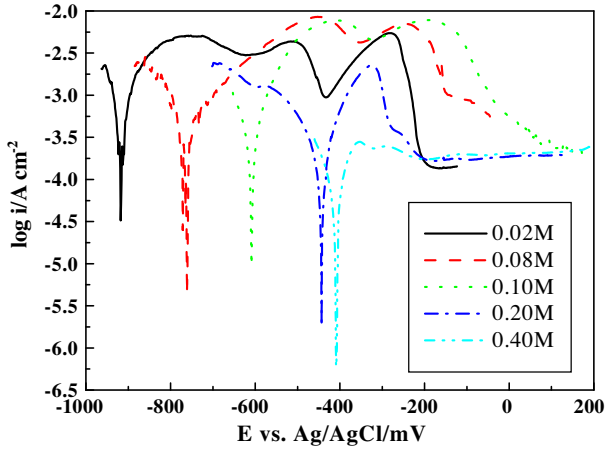

Figure 6 log *i–E* curves of Zn–Ni–Fe alloy, electrodeposited on steel from a bath containing 0.10 M $ZnSO_4$, 0.10 M $NiSO_4$, 0.01 M H_2SO_4, 0.20 M Na_2SO_4, 0.20 M H_3BO_3 with different concentrations of $FeSO_4$ at 5 mA cm^{-2} for 10 min at 30 °C, in 50 cm^3 0.05 M HCl at 30 °C.

alloys. It is observed that, at low Fe^{2+} concentration in the plating bath, the measured corrosion potential has a more negative value and the alloy has low corrosion resistance. As the Fe^{2+} concentration has increased, the measured corrosion potential has shifted to more noble potential due to the decrease of pure Zn relative to the increase in γ-Ni_2Zn_{11} and Fe_3Ni_2 contents in the deposit.

Concomitant changes in the structure and morphology can be observed from the SEM analysis that depends strongly on the iron concentration in the electrolytic bath. Fig. 7a shows the SEM image of Zn–Ni deposits which had coarse grain size while Fig. 7b and c shows the surface morphology of Zn–Ni–Fe electrodeposits at different Fe^{2+} concentrations. The ternary Zn–Ni–Fe deposits demonstrate a homogenous structure form of crystallites, and the grain size is finer. Moreover, it is found that the grain size decreases and gives more compact and smooth morphology with increasing nickel and iron contents in the ternary Zn–Ni–Fe deposits.

The effects of Fe^{2+} concentrations on the percentage of Zn, Ni and Fe in Zn–Ni–Fe alloys from the sulfate bath are shown in Table 1. Addition of iron sulfate, zinc content and amount in the deposit generally decreased. But, iron and nickel contents and amounts in the deposit increased under the same conditions. While iron content in the deposit is 1.7% in the presence of 0.10 M $FeSO_4$, the alloy iron content increases to reach 4.1%, when its concentration was 0.40 M in the bath. The influence of iron ion concentration on the cathodic current efficiency of Zn–Ni–Fe alloys was also calculated. It can be

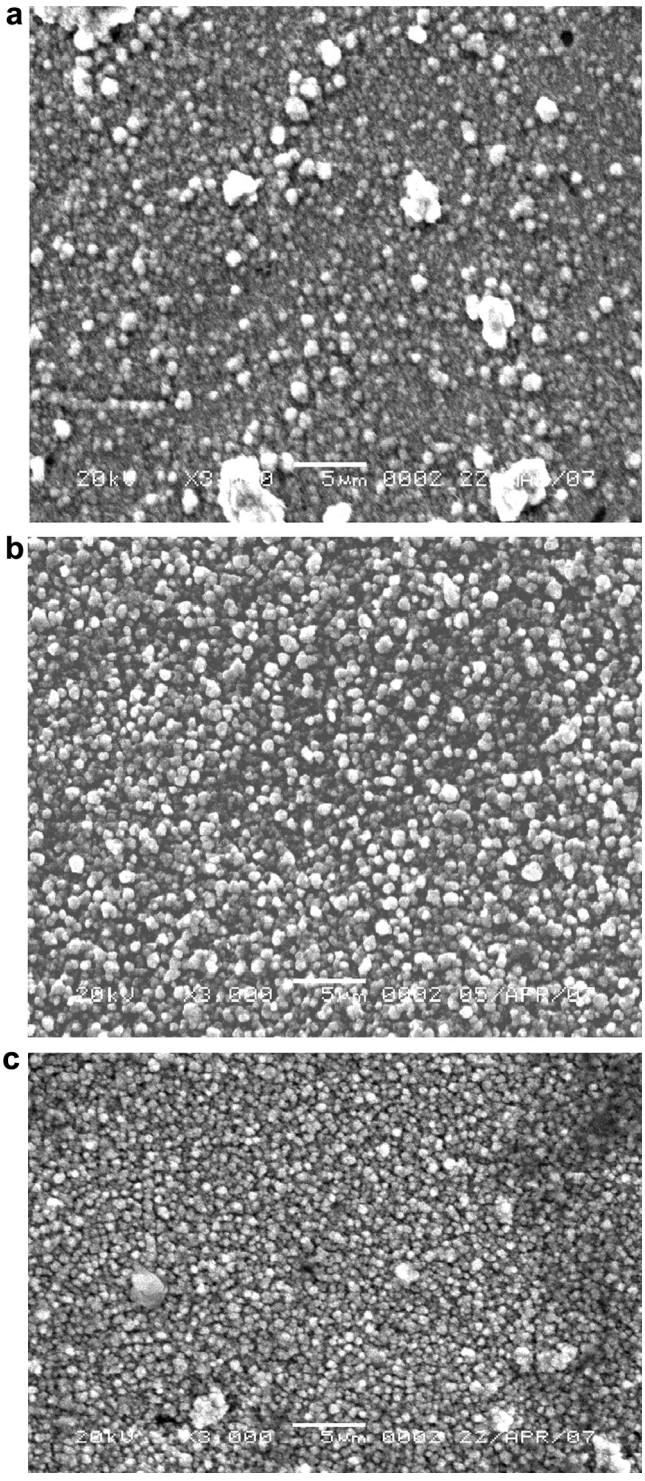

Figure 7 SEM photograph of electrodeposited Zn–Ni–Fe alloy on steel from a bath containing 0.10 M ZnSO4, 0.10 M $NiSO_4$, 0.01 M H_2SO_4, 0.20 M Na_2SO_4, 0.20 M H_3BO_3 with different concentrations of $FeSO_4$ at 5 mA cm^{-2} for 10 min at 30.0 °C (a) 0.0 M FeSO4, (b) 0.1 M $FeSO_4$ and (c) 0.4 M $FeSO_4$.

seen that Zn–Ni–Fe alloy current efficiency decreased with increasing the molar percentage of Fe^{2+} in the bath.

The influence of iron incorporation into Zn–Ni–Fe deposits on the corrosion behavior of the coatings was studied. The corrosion potential ($E_{corr.}$) is, however, an indication of the activity of the deposit in a corrosive environment. It was found that the corrosion potential $E_{corr.}$ (Table 1) shifts toward more positive values as the iron percentage in the deposit increased. It is also clear, that at much higher Fe^{2+} concentrations the corrosion potential shifts to much more noble direction than that at low concentrations, and this may be attributed to the formation of Fe_3Ni_2 phase in the deposit. Also, it is clear that the polarization resistance of the deposit increased with increasing Ni content of the alloy, but the corrosion current and the thickness were decreased. Decrease of the deposited thickness is perhaps related to the decrease of Zn content in the alloy, which represents the main alloy component of low density.

3.2. Effect of deposition time on Zn–Ni–Fe alloy deposition

Fig. 8a shows the cyclic voltammetric behavior of the studied alloys by using different high sweeping rates (low deposition time from 15–40 s). It is obvious from the cathodic part of these curves that the height of the cathodic peak, which starts approximately at −577 mV, rose up when the sweeping rate increases (the deposition time decreases). It appears that the height of the first and second anodic peaks has decreased when the deposition time increases (15–40 s), owing to the decrease of γ-Ni_2Zn_{11} and Fe_3Ni_2 phases as a result of the decrease of Zn and Fe concentrations in the deposit, which will aid to decrease the corrosion resistance of the deposit. At very low deposition time (15 s), the deposit is enriched with the formed phases, which will be indicated by high corrosion resistance comparable to higher time (40 s). Increasing the deposition time reveals generally an increase in the final peak, but not compensating the decrease in the other constituents owing to decrease the corrosion resistance.

However, Fig. 8b shows the cyclic voltammetric behavior of the studied alloys at different low sweeping rates (high deposition time from 1 to 30 min). The voltammograms in this figure consist of three anodic peaks. The first anodic peak was seen at −884 mV, its peak height increases (1–10 min) and then decreases (10–30 min) with increasing deposition time. The second peak has appeared at about −708 mV and is attributable to the dissolution of zinc from (γ-Ni_2Zn_{11}) phase, which overlaps with the dissolution of iron from (Fe_3Ni_2) phase; its height decreases with increasing the deposition time. The height of the third anodic peak at more noble potentials, −321 mV corresponds to the dissolution of nickel from its phases, increased with increasing the deposition time. These results are due to the increase of the content of Ni^{2+} and Zn^{2+} with the passing time.

The anodic linear sweep voltammograms obtained during the dissolution of the deposit (Fig. 9) show the phase structures of Zn–Ni–Fe alloys that deposited using different deposition times. Based on ALSVs, an identification of the phase structures present in the Zn–Ni–Fe alloys was made previously. From the figure it is seen that at a deposition time of 60 s, there are very small anodic dissolution peaks, indicating the presence of only two phases that may be the pure Zn-phase and the γ-Ni_2Zn_{11} phase. With increasing deposition time the height of the peaks increase, indicating an increase in the amount of the alloy constituents (Table 2). Moreover, the anodic peaks shift to the positive direction, giving rise to an increment in the content of the nobler component of the alloy, (i.e., Ni and Fe) related to the increase of the Zn amount.

Table 1 Values of Zn, Ni and Fe amount in the deposit, total mass of the deposit, % (Zn, Ni and Fe content), current efficiencies, % (Zn–Ni–Fe deposit) and thickness of the deposit on copper (2 cm^2), deposited galvanostatically from a bath containing 0.10 M $ZnSO_4$, 0.10 M $NiSO_4$, different concentrations of $FeSO_4$, 0.01 M H_2SO_4, 0.20 M Na_2SO_4 and 0.20 M H_3BO_3 at 5 mA cm^{-2} for 10 min at 30.0 °C, and electrochemical corrosion measurements of the same deposit on steel (0.196 cm^2).

Parameter	Fe^{2+} conc. (M)				
	0.02	0.08	0.1	0.2	0.4
Zn amount in the deposit (10^{-5} g)	163	147	126	115	102
Ni amount in the deposit (10^{-5} g)	9.3	13.3	16.5	18.8	20.5
Fe amount in the deposit (10^{-5} g)	0.81	1.19	2.4	3.5	5.2
Total mass of the deposit (10^{-5} g)	173	162	145	137	128
Zn content (%)	94	90.9	86.9	83.7	79.8
Ni content (%)	5.4	8.3	11.4	13.7	16.1
Fe content (%)	0.5	0.7	1.7	2.5	4.1
Zn–Ni–Fe deposit current efficiency ($e_{Zn-Ni-Fe}$) (%)	85.7	80.3	72.4	68.9	64.4
Thickness of the deposit (μm)	1.2	1.11	1.1	0.92	0.85
R_p (k Ω)	0.10	0.15	0.194	0.36	0.56
I_{corr} (A $cm^{-2} \times 10^{-5}$)	1.67	1.45	1.27	1.14	1.10
(E_{corr}) Corrosion potential (mV)	−920	−758	−608	−442	−406

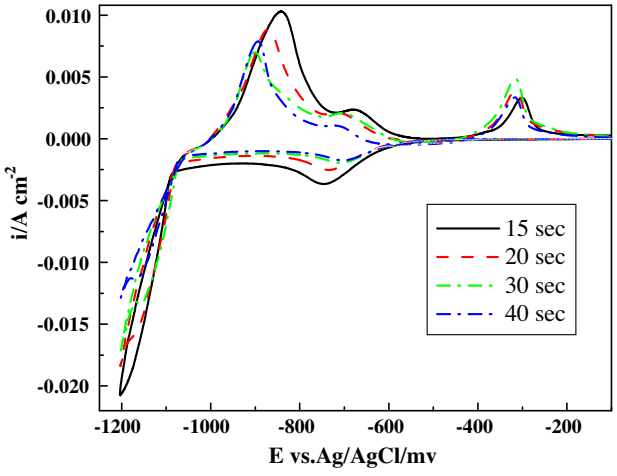

Figure 8a *i–E* curves (cyclic voltammograms) for steel in 0.10 M $ZnSO_4$, 0.10 M $NiSO_4$, 0.10 M $FeSO_4$, 0.01 M H_2SO_4, 0.20 M Na_2SO_4 and 0.20 M H_3BO_3 at 30.0 °C and high scan rate.

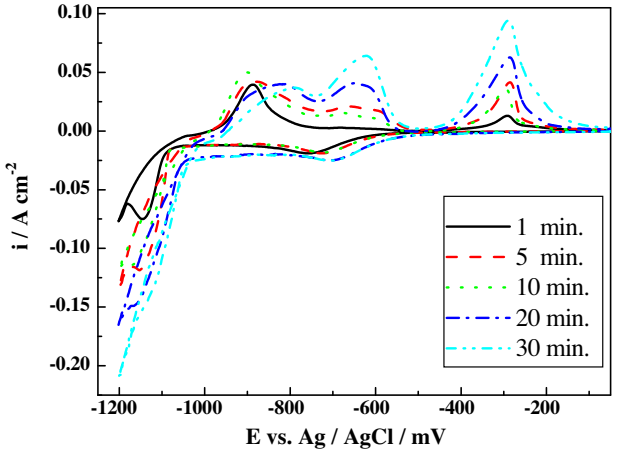

Figure 8b *i–E* curves (cyclic voltammograms) for steel in 0.10 M $ZnSO_4$, 0.10 M $NiSO_4$, 0.10 M $FeSO_4$, 0.01 M H_2SO_4, 0.20 M Na_2SO_4 and 0.20 M H_3BO_3 at 30.0 °C and low scan rate.

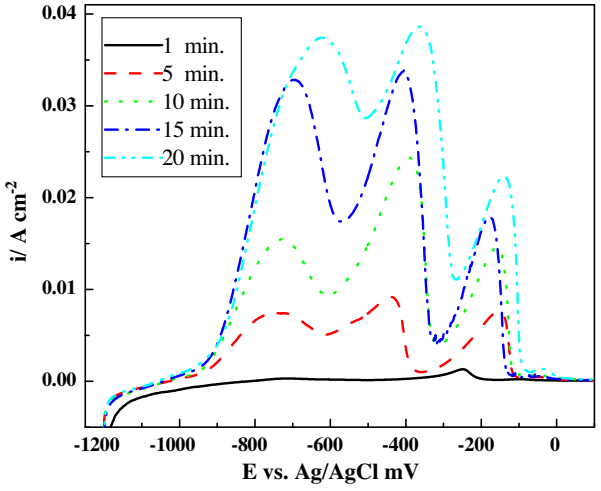

Figure 9 ALSVs of Zn–Ni–Fe alloy, electrodeposited on steel from a bath containing 0.10 M $ZnSO_4$, 0.10 M $NiSO_4$, 0.10 M $FeSO_4$, 0.01 M H_2SO_4, 0.20 M Na_2SO_4 and 0.20 M H_3BO_3 at 5 mA cm^{-2} for different times, in 0.5 M Na_2SO_4 + 0.05 M EDTA solution at scan rate 5 mV s^{-1} and 30 °C.

This is in accordance with the results shown in Table 2, according to which an increase of deposition time results in an increase of the alloy constituents. Co-deposition of Fe with lower amount appears at lower deposition time and slightly increases with increasing the deposition time (Table 2). In addition, as can be seen from the figure that the Fe dissolution peak does not appear at high deposition time although it exists in the deposit (Table 2). This is not due to the non-co-deposition of Fe but the interference, between the two peaks concerning the dissolution of Zn and Fe, respectively (the lower Fe content relative to higher Zn content), causes overlapping which gives rise to only one anodic peak that appears at nobler potential.

Linear polarization resistance tests (Fig. 10a) have been done using steel-coated galvanostatically by Zn–Ni–Fe alloys. It is clear that, at deposition time (10–50 s) the measured

Table 2 Values of Zn, Ni and Fe amount in the deposit, total mass of the deposit, % (Zn, Ni and Fe content) and thickness of the deposit on copper (2 cm^2), deposited galvanostatically from a bath containing 0.10 M $ZnSO_4$, 0.10 M $FeSO_4$, 0.10 M $NiSO_4$, 0.01 M H_2SO_4, 0.20 M Na_2SO_4 and 0.20 M H_3BO_3 at 5 mA cm^{-2} and 30.0 °C for different deposition times, and electrochemical corrosion measurements of the same deposit on steel (0.196 cm^2).

Parameter	Time (min)				
	5	10	15	20	30
Zn amount in the deposit (10^{-5} g)	68.1	126	207	233	354
Ni amount in the deposit (10^{-5} g)	7.5	16.5	26.3	39.5	57.1
Fe amount in the deposit (10^{-5} g)	2	2.5	3.55	5.41	6.93
Total mass of the deposit (10^{-5} g)	77.6	145	237	278	418
Zn content (%)	87.7	86.98	87.37	83.84	84.68
Ni content (%)	9.6	11.3	11.12	14.20	13.65
Fe content (%)	2.6	1.7	1.49	1.94	1.65
Thickness of the deposit (μm)	0.53	1.1	1.61	1.88	2.83
R_p (k Ω)	0.145	0.194	0.274	0.285	0.318
I_{corr} (A $cm^{-2} \times 10^{-4}$)	0.138	0.127	0.115	0.105	0.096
(E_{corr}) Corrosion potential (mV)	−634	−608	−597	−518	−394

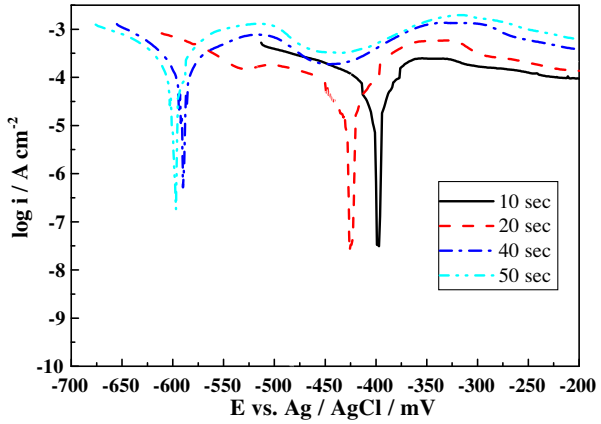

Figure 10a log *i*–*E* curves of Zn–Ni–Fe alloy, electrodeposited on steel from a bath containing 0.10 M $ZnSO_4$, 0.10 M $NiSO_4$, 0.10 M $FeSO_4$, 0.01 M H_2SO_4, 0.20 M Na_2SO_4 and 0.20 M H_3BO_3 at 5 mA cm^{-2} for different times, in 50 cm^3 0.05 M HCl at 30 °C.

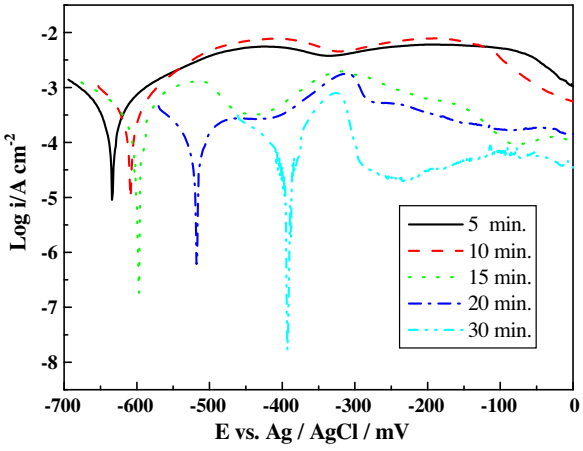

Figure 10b log *i*–*E* curves of Zn–Ni–Fe alloy, electrodeposited on steel from a bath containing 0.10 M $ZnSO_4$, 0.10 M $NiSO_4$, 0.10 M $FeSO_4$, 0.01 M H_2SO_4, 0.20 M Na_2SO_4 and 0.20 M H_3BO_3 at 5 mA cm^{-2} for different times, in 50 cm^3 0.05 M HCl at 30 °C.

corrosion potentials are more positive and the alloy has a better corrosion resistance; this may be due to the presence to the highly stable γ-Ni_2Zn_{11} phase. As the deposition time has increased, the $E_{corr.}$ shifted negatively due to the decrease of γ-phase content in the deposit during this range of time. However, the increase of the deposition time from 5 to 30 min

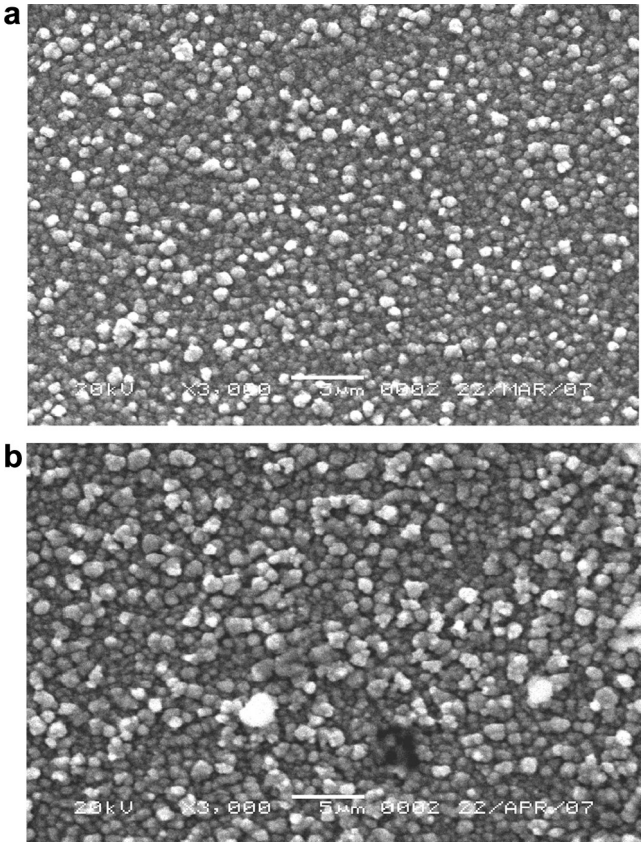

Figure 11 SEM photograph of electrodeposited on steel from a bath containing 0.10 M $ZnSO_4$, 0.10 M $NiSO_4$, 0.10 M $FeSO_4$, 0.01 M H_2SO_4, 0.20 M Na_2SO_4 and 0.20 M H_3BO_3 at 5 mA cm^{-2} for different times (a) 10 min and (b) 30 min.

(Fig. 10b), shifts the measured corrosion potential toward positive direction. This may be due to the increase of the amounts of the alloy constituents by increasing the deposition time. The obtained data from Table 2 show that the thickness of the deposited layer has increased (0.53–2.83 μm) when the deposition time increases (5–30 min). On the other hand, Table 2 also shows that the corrosion potential and current have decreased and the polarization resistance has increased as the deposition time increases.

Fig. 11a and b shows the influence of the deposition time on Zn–Ni–Fe deposits morphology. Deposits obtained at 10 min. show to be uniform; the phases are homogeneous and have a rough surface (Fig. 11a). With further increases of the deposition time (30 min) compact deposits with homogeneous structure morphology were obtained (Fig. 11b).

4. Conclusions

In the present investigation, the electrodeposition operating conditions for Zn–Ni–Fe alloys from sulfate baths and their corrosion resistance were studied. The obtained results revealed that the ternary Zn–Ni–Fe deposits exhibit higher corrosion resistance in comparison with Zn–Ni deposits. The increasing corrosion resistance of ternary deposits is not only attributed to the formation of (γ-Ni_2Zn_{11}) phase, but also to iron co-deposition and the formation of (Fe_3Ni_2) phase. It is interesting to mention that the current efficiency of Zn–Ni–Fe alloy decreases as a result of increasing Fe^{2+} concentration from 0.02 to 0.4 M.

The results also revealed that the deposition time has a great effect on the electrodeposition of Zn–Ni–Fe alloy and consequently the corrosion resistance of the formed deposit. The increasing of deposition time results in an increase of the alloy constituents and in turn the corrosion resistance of the electrodeposit alloy. Co-deposition of Fe with lower amount appears at lower deposition time and slightly increases with increasing the deposition time.

References

Abou-Krisha, M.M., 2005. Appl. Surf. Sci. 252, 1035.

Abou-Krisha, M.M., Rageh, H.M., Matter, E.A., 2008. Surf. Coat. Technol. 202, 3739.

Ananth, M.V., Parthasaradhy, N.V., 1997. Int. J. Hydrogen Energy 22, 747.

Ashassi-Sorkhabi, H., Hagrah, A., Parvini-Ahmadi, N., Manzoori, J., 2001. Surf. Coat. Technol. 140, 278.

Brenner, A., 1963. In: Electrodeposition of Alloys, vol. 2. Academic Press, New York, p. 194.

Chitharanjan Hegde, A., Venkatakrishna, K., Eliaz, N., 2010. Surf. Coat. Technol. 205, 2031.

Eliaz, N., Venkatakrishna, K., Chitharanjan Hegde, A., 2010. Surf. Coat. Technol. 205, 1969.

Ganesan, Prabhu, Kumaraguru, Swaminatha, Popov, Branko, 2007. Surf. Coat. Technol. 201, 7896.

Hu, Weikang, 2000. Int. J. Hydrogen Energy 25, 111.

Li, Hongqi, Feng Jiang, Ni, Song, Li, Li, Sha, Gang, Liao, Xiaozhou, Ringer, Simon P., Choo, Hahn, Liawb, Peter K., Misraa, Amit, 2011. Scripta Mater. 65, 1.

Liu, Yichun, Liu, Lei, Shena, Bin, Hu, Wenbin, 2011. Mater. Sci. Eng. A 528, 5701.

Ortiz, Z.I., Diaz-Arista, P., Meas, Y., Ortega-Borges, R., Trejo, G., 2009. Corros. Sci. 51, 2703.

Safranekv, W.H., 1986. The Properties of Electrodeposited Metals and Alloys. AESF, Orlando, FL, p. 466.

Tian, Liangliang, Xu, Jincheng, Qiang, Chengwen, 2011. Appl. Surf. Sci. 257, 4689.

Veeraraghavan, Basker, Kim, Hansung, Popov, Branko, 2004. Electrochim. Acta 49, 3143.

Vlad, L., Pascariu, P., Tanase, S.I., Pinzaru, D., Dobromir, M., Nica, V., Georgescu, V., 2011. Physica B 406, 1481.

Yogesha, S., Chitharanjan Hegde, A., 2011. Mater. Sci. Eng. A 211, 1409.

Younan, M.M., Oki, T., 1996. J. Appl. Electrochem. 26, 537.

Zhang, Z., Leng, W.H., Shao, H.B., Zhang, J.Q., Wang, J.M., Cao, C.N., 2001. J. Electroanal. Chem. 516, 127.